

Link between the superconducting dome and spin-orbit interaction in the (111) $\text{LaAlO}_3/\text{SrTiO}_3$ interface

P. K. Rout, E. Maniv, and Y. Dagan

Raymond and Beverly Sackler School of Physics and Astronomy, Tel-Aviv University, Tel Aviv, 69978, Israel

(Dated: April 4, 2025)

We measure the gate voltage (V_g) dependence of the superconducting properties and the spin-orbit interaction in (111) oriented $\text{LaAlO}_3/\text{SrTiO}_3$ interface. Superconductivity is observed in a dome-shaped region in the carrier density-temperature phase diagram with the maxima of superconducting transition temperature T_c and the upper critical fields lying at the same V_g . The spin-orbit interaction determined from the superconducting parameters and confirmed by weak-antilocalisation measurements follows the same gate voltage dependence as T_c . The correlation between superconductivity and spin-orbit interaction as well as the enhancement of parallel upper critical field, well beyond the Chandrasekhar-Clogston limit suggest that superconductivity and the spin-orbit interaction are linked in a non-trivial fashion. We propose possible scenarios to explain this unconventional behavior.

Oxide heterostructure provides a unique platform where various degrees of freedom from the constituent materials can combine such that new collective phenomena emerge at the interfaces [1]. An interesting example is two dimensional (2D) electron liquid at the interface between (100) oriented SrTiO_3 and LaAlO_3 that exhibits gate tunable superconductivity [2, 4, S1] and spin-orbit interaction [4, 6, S2]. Recent experiments on the (111) $\text{LaAlO}_3/\text{SrTiO}_3$ have shown 2D conduction [7–9] and superconductivity with transition temperature (T_c) of about 100 mK [10, 11]. In (111) oriented $\text{LaAlO}_3/\text{SrTiO}_3$ interface, the cubic lattice is projected onto the (111) plane of the interface resulting in a 2D six-fold crystalline structure. Angle resolved photoemission studies on (111) SrTiO_3 surface reveal a six-fold symmetric electronic structure [12, 13]. This 2D crystalline symmetry is also reflected in the magneto-transport properties [9] and has been predicted to host exotic electronic orders [14–17]. At low temperatures this symmetry is lowered since bulk SrTiO_3 undergoes multiple structural transitions. Below 105 K a transition from cubic to tetragonal phase occurs [18]. The symmetry is further reduced to triclinic below ~ 70 K and polar domain walls where inversion symmetry is broken are created [19]. Such a domain wall can be pinned to the interface resulting in unconventional superconductivity, which is linked the spin-orbit coupling.

In a 2D superconductor, for a magnetic field applied perpendicular to the superconducting plane, superconductivity is broken when vortices become closely packed. By contrast, the parallel upper critical field ($H_{c\parallel}$) is determined by the Chandrasekhar-Clogston limit [20, 21], which is set by comparing the Zeeman energy to the superconducting gap. In the presence of spin-orbit interaction this upper bound is relaxed [22, 23].

In this letter we report a nonmonotonic (dome-shaped) dependence of T_c with gate voltage in the (111) $\text{SrTiO}_3/\text{LaAlO}_3$ interfaces. From the gate dependence of T_c and $H_{c\parallel}$ we estimate the spin-orbit energy (ε_{SO}), which follows the nonmonotonic behavior of T_c . Remarkably, we found similar behavior for the spin-orbit field

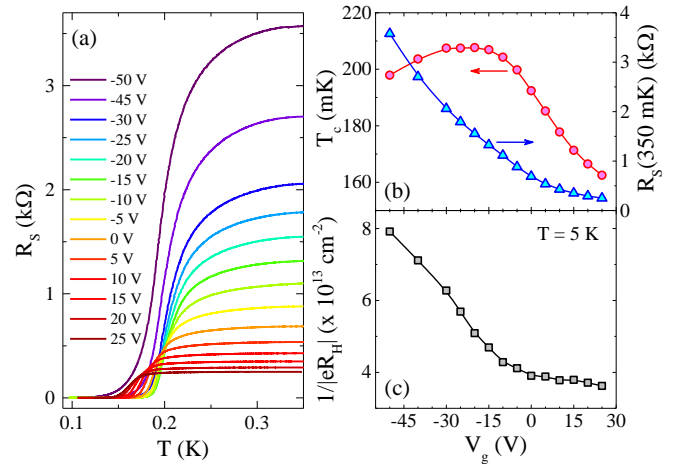


FIG. 1. (a) Temperature dependence of sheet resistance R_S (T) for various gate voltages. (b) T_c and R_S (350 mK) as a function of V_g . (c) Gate dependence of the inverse Hall coefficient $1/|eR_H|$ at $T = 5 \text{ K}$.

H_{SO} extracted from weak antilocalisation measurements.

Epitaxial films of LaAlO_3 were deposited on atomically flat SrTiO_3 (111) substrate using pulsed laser deposition. The details of deposition procedure and substrate treatment are described in Ref. [9]. We control the layer-by-layer growth of 14 monolayers (LaO_3/Al layers) by reflection high energy electron diffraction RHEED oscillations. The atomic force microscope images show the step and terrace morphology of the film with step heights of 0.22 nm. The electrical measurements with the current along $[11\bar{2}]$ direction were carried out in Leiden Cryogenics custom made dilution refrigerator.

Figure 1 (a) presents the temperature dependent sheet resistance R_S (T) at various gate voltages, V_g . A clear gate dependent superconducting transition is observed. We define the critical temperature T_c as the temperature at which R_S reaches half of its value at 350 mK. The normal state resistance R_S (350 mK) decreases mono-

tonically with increasing V_g [Fig. 1 (b)], which is consistent with previous reports [8, 9]. The monotonic increase of R_S is contrasted with the nonmonotonic dependence of T_c on V_g . Similar dome-shaped region in the carrier density-temperature phase diagram is seen in many unconventional superconductors and in the (100) $\text{LaAlO}_3/\text{SrTiO}_3$ interface.

In the (100) $\text{LaAlO}_3/\text{SrTiO}_3$ interface the Hall coefficient depends nonmonotonically on gate voltage. Surprisingly, this nonmonotonic behaviour is also seen in the gate dependence of the quantum oscillations (SdH) frequency. Both SdH frequency and low field inverse Hall coefficient follow the gate dependence of T_c for the (100) interface [24, S1] or the superconductivity starts appearing when low field inverse Hall coefficient decreases from its maximum value [25]. By contrast, for the (111) interface the inverse Hall coefficient monotonically decreases with V_g [Fig. 1 (c)] consistent with previous observations [8, 9]. In case of the (111) $\text{LaAlO}_3/\text{SrTiO}_3$ interface the titanium t_{2g} bands are split into low and high spin states due to the atomic spin-orbit interaction [14, 15]. We have shown that the lower spin state is first populated when accumulating electrons with increasing V_g [9]. This two band scenario complicates the interpretation of the Hall data. We have estimated the amount of carrier density modulation due to electric field effect similar to Ref. [2, 26]. Since the V_g range used is relatively small, the nonlinearities in the dielectric constant (ϵ) can be neglected and thus the corresponding modulation of electron density is $\simeq 1.3 \times 10^{13} \text{ cm}^{-2}$ with $\epsilon \simeq 15000$. This value is much smaller than net change in $1/|eR_H|$ of $\simeq 4.3 \times 10^{13} \text{ cm}^{-2}$. Moreover, the electron density due to field effect increases with V_g in contrast to the observed behaviour in Fig. 1 (c). All these observations indicate the presence of an hole band in addition to electron band(s) in (111) interface. We have confirmed this scenario by analysing the normal state transport data via a simplistic non-interacting two band model with one hole and one electron band (See Ref. [27] for more details). Therefore, It is possible that hole contribution to the electronic transport (and perhaps to superconductivity) becomes important in this V_g range [8]. This is also consistent with the polar structure of the (111) interface [7].

The sheet resistance versus magnetic field at 90 mK for various gate voltages is plotted in Fig. 2 (a, b) for perpendicular and parallel field configurations, where the sample is properly aligned with the field within an accuracy of 2° . We define the critical field ($H_{c\perp}$) for perpendicular magnetic field configuration such that $R_S(H_{c\perp}) = R_S(350 \text{ mK})/2$ and a similar criterion is followed for $H_{c\parallel}$ [28]. In Fig. 2 (c) we plot $H_{c\parallel}$ and $H_{c\perp}$ as a function of V_g both exhibiting nonmonotonic behavior with the maximum at the same gate voltage as T_c . $H_{c\parallel} > H_{c\perp}$ for all gate voltages reaching a maximal ratio of ~ 16 . Such strong anisotropy between two field orientations is an evidence for 2D superconductivity in the (111) interface. Thus, it is expected that the superconducting layer thick-

ness (d) should be smaller than the Ginzburg-Landau coherence length (ξ_{GL}). To check this, we extract ξ_{GL} from $H_{c\perp}$ using the relation: $\xi_{GL} = \sqrt{\Phi_0/2\pi H_{c\perp}}$. It is presented in Fig. 2 (d) together with its extrapolation to zero temperature using $H_{c\perp}(T) = H_{c\perp}(0)(1 - T/T_c)$ valid for a 2D superconductor. Since parallel magnetic field fully penetrates a 2D ($d \ll \xi$) superconductor we can only estimate the upper limit for d denoted as \bar{d} , which can be found from $\bar{d} = \sqrt{3}\Phi_0/\pi\xi_{GL}H_{c\parallel}$ [See Fig. 2 (d)]. We note that, for all V_g , $\bar{d} < \xi_{GL}(0)$ rendering superconductivity in the (111) $\text{SrTiO}_3/\text{LaAlO}_3$ two dimensional.

For parallel field configuration in a 2D superconductor the orbital motion and vortices can be neglected making the Zeeman energy the dominant pair-breaking effect. This leads to an upper (Chandrasekhar-Clogston) limit of $H_{c\parallel}$ given by $H_P = 3.5k_B T_c / \sqrt{2}g\mu_B$ (μ_B is the Bohr magneton) in BCS weak coupling limit [20, 21]. Assuming gyromagnetic ratio $g \simeq 2$, we observe $H_{c\parallel} > H_P$ for all gate voltages reaching a maximal ratio of ~ 11 [Fig. 2 (c)]. In the presence of strong spin-orbit coupling the Chandrasekhar-Clogston limit can be relaxed. Other reasons for breaking of this limit could be strong coupling superconductivity, many body effects and anisotropic pairing mechanism.

To determine the spin-orbit interaction from $H_{c\parallel}$ we use a somewhat oversimplified picture of spin-orbit scattering that suppresses spin orientation by the Zeeman field [22]. For strong spin-orbit interaction $H_{c\parallel}$ can be expressed in terms of the spin-orbit energy (ε_{SO}) as: $H_{c\parallel} = 0.602\sqrt{\varepsilon_{SO}/k_B T_c} H_P$ with $\varepsilon_{SO} = \hbar/\tau_{SO}$ and τ_{SO} is the spin-orbit scattering time. Remarkably, this analysis reveals a nonmonotonic dependence of ε_{SO} on V_g as shown in Fig. 3 (b). This is the main finding of our paper. For the (110) $\text{LaAlO}_3/\text{SrTiO}_3$ gate independent spin-orbit coupling has been observed [29]; perhaps because of the nonpolar structure of this interface. The findings on the (110) interface are contrasted with our results of strong and gate-tunable spin-orbit interaction for the (111) interface that follows the behavior of the superconducting dome. A weaker correlation between spin-orbit coupling and T_c in the (100) interface can be deduced by combining Refs. [4, 6, S2], where $H_{c\parallel}$ is smaller.

To further confirm the presence of spin-orbit interaction we studied the perpendicular magnetoresistance well above T_c at 1.3 K [Fig. 3 (a)]. For a 2D diffusive metallic system placed in a perpendicular magnetic field (H), the field dependent quantum correction to conductivity $\Delta\sigma(H)$ normalised by quantum conductance

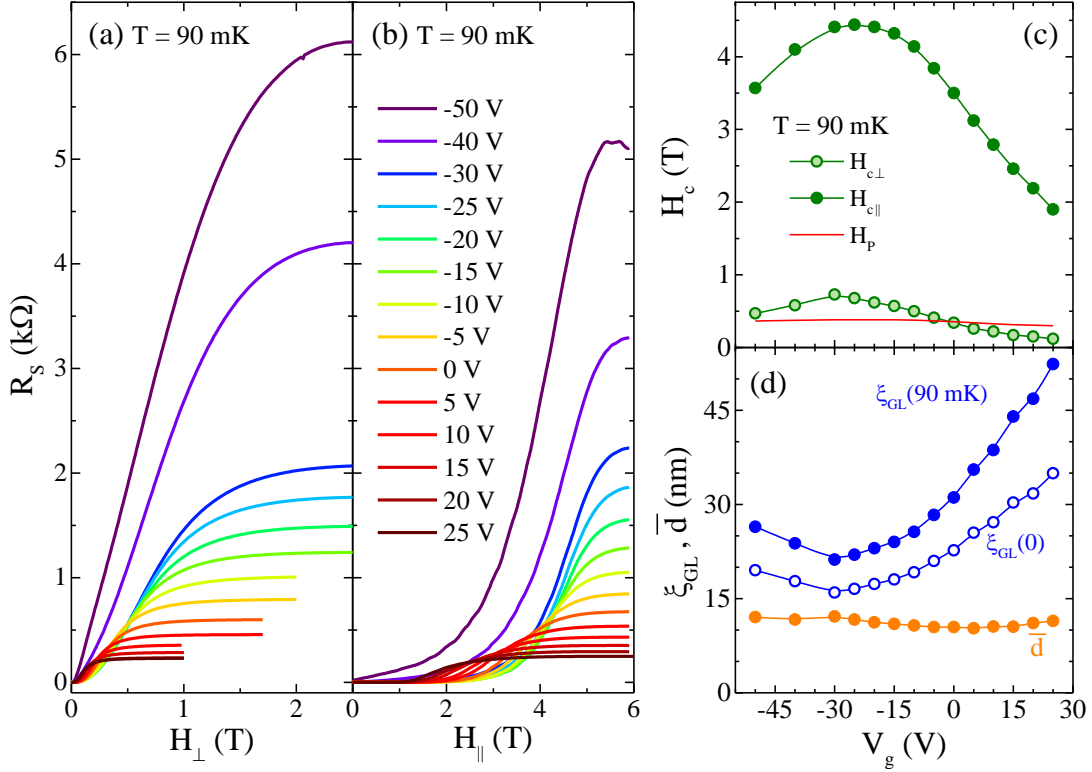


FIG. 2. Magnetoresistance $R_S(H)$ at $T = 90$ mK in (a) perpendicular (\vec{H} perpendicular to the current and interface) and (b) longitudinal (\vec{H} parallel to the current and interface) configurations for various V_g . (c) $H_{c\perp}$ and $H_{c\parallel}$ at 90 mK as a function of V_g along with Chandrasekhar-Clogston limit H_P . (d) Gate dependence of ξ_{GL} (90 mK), $\xi_{GL}(0)$, and \bar{d} .

($\sigma_0 = e^2/\pi h$) can be expressed as [30, S2]:

$$\begin{aligned} \frac{\Delta\sigma(H)}{\sigma_0} = & \Psi\left(\frac{H}{H_i + H_{SO}}\right) \\ & + \frac{1}{2\sqrt{1-\gamma^2}}\Psi\left(\frac{H}{H_i + H_{SO}(1 + \sqrt{1-\gamma^2})}\right) \\ & - \frac{1}{2\sqrt{1-\gamma^2}}\Psi\left(\frac{H}{H_i + H_{SO}(1 - \sqrt{1-\gamma^2})}\right) \\ & - \frac{AH^2}{1 + CH^2}. \end{aligned} \quad (1)$$

where $\Psi(x) = \ln(x) + \psi(\frac{1}{2} + \frac{1}{x})$ [$\psi(x)$ is the digamma function] and $\gamma = g\mu_B H/4eDH_{SO}$ (D is the diffusion coefficient). H_i and H_{SO} are the inelastic and spin-orbit fields, respectively. The classical orbital magnetoresistance contributes a Kohler term to Eq. (1) with the parameters A and C . Figure 3 (c) shows H_i and H_{SO} for different V_g (See supplemental material for the gate dependence of g , A and C [27]). Clearly, $H_{SO} > H_i$ for all V_g suggesting that we are in the weak antilocalisation regime [See Fig. 3 (a)]. H_{SO} from weak antilocalisation [Fig. 3 (c)] shows nonmonotonic behavior similar to ε_{SO} inferred from superconductivity [Fig. 3 (b)] and, furthermore, they have maximum value at the same gate voltage

as T_c .

In general, the $\text{LaAlO}_3/\text{SrTiO}_3$ interface has a complicated band structure involving multiple contributions from the titanium d -bands [31, 32]. Therefore, the extracted parameters from weak antilocalisation do not correspond to an individual band; instead an averaged value over all the bands should be considered [33]. We have extracted various averaged time scales, i. e. τ_{SO} , τ_i (inelastic time), and τ (elastic scattering time) [Fig. 3 (d)]. The $\tau_{SO(i)}$ are related to $H_{SO(i)}$ determined from weak-antilocalisation as: $H_{SO(i)} = \hbar/4eD\tau_{SO(i)}$. The effective diffusion coefficient (D) and τ are calculated using a naïve Drude model for a 2D electron gas (See Ref. [27]). Using this analysis we find that τ_{SO} depends linearly on τ^{-1} for $V_g < -25$ V [See the inset of Fig. 3 (d)] while for $V_g > -25$ V both τ_{SO} and τ increase with V_g [Fig. 3 (d)].

The low V_g regime ($V_g < -25$ V) is governed by a D'yakonov-Perel'-type spin-orbit relaxation mechanism for which $\tau_{SO} \propto \tau^{-1}$. In this scenario the electron precesses around the spin-orbit field, which is changing due to momentum scattering at a typical time τ [34]. The high V_g regime, on the other hand, is characterized by $\tau_{SO} \propto \tau$, suggesting that the electron spin is coupled to the crystal momentum. Interestingly these two regimes separated by the point where $\tau_{SO} \simeq \tau$ and the maxi-

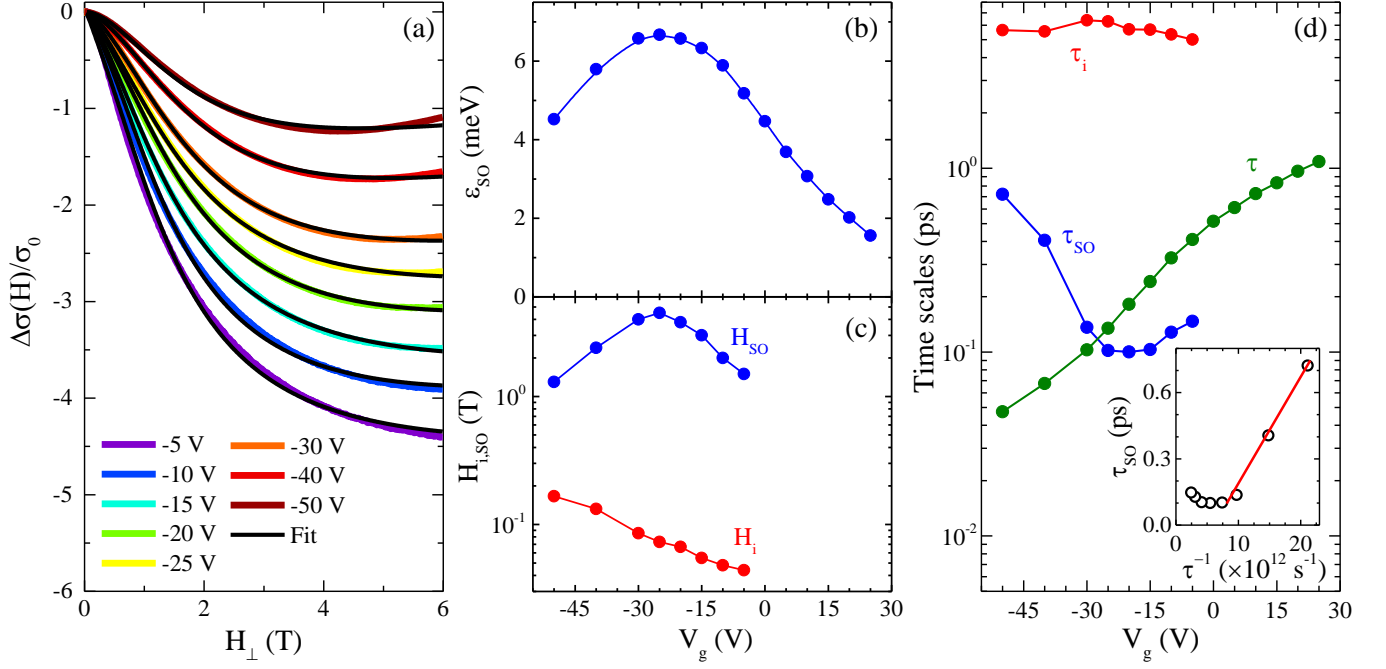


FIG. 3. (a) The normalised perpendicular magnetoconductance $\Delta\sigma(H)/\sigma_0$ for different V_g at $T = 1.3$ K. The black solid lines are the fits according to Eq. 1. (b) ϵ_{SO} as a function of V_g determined from $H_{c\parallel}$ (See text for more details). (c) Gate dependence of H_i and H_{SO} extracted from the fitting of weak antilocalisation. (d) Gate dependence of τ_i , τ_{SO} , and τ . Inset shows τ_{SO} as a function of τ^{-1} along with the solid line as guide to the eye.

imum of T_c (and $H_{c\parallel}$) dome lies close to this V_g . All these observations suggest the mixing of multiple bands in the presence of strong spin-orbit interaction for higher V_g . This scenario concurs with our recent report of crystalline six-fold anisotropic magnetoresistance in the (111) interfaces [9], where the six-fold term appears as a result of another band with higher spin state J getting populated with increasing V_g . It is therefore possible that the crystalline spin-orbit interaction becomes important close to this avoided band crossing region due to the orbital mixing [23, 35]. This interaction becomes smaller as V_g is further increased away from the band crossing regime resulting in a dome in the spin-orbit energy versus V_g . Such multiband effect can also lead to dome shaped superconductivity with maximum T_c lying at this regime [as observed in Fig. 1 (b)] similar to the case for (100) interface [S1]. A more exotic mechanism of superconductivity in $\text{LaAlO}_3/\text{SrTiO}_3$ interface involves the formation of Fulde-Ferrell-Larkin-Ovchinnikov (FFLO) state due to large spin-orbit coupling [36]. This can somewhat explain nonmonotonic gate dependence of $H_{c\parallel}$ and T_c with the maxima lying at $\tau_{SO} = \tau$. However, the $H_{c\parallel}$ for a quasi-2D superconductor in FFLO state is estimated to be at most 2.5 times the Chandrasekhar-Clogston limit [37], which is much lower than the observed values [See Fig. 2 (c)]. Therefore, full theoretical understanding of the phenomenological link observed here between the superconducting dome and the spin-orbit energy is yet to

be developed.

Salje *et al.* have found that for SrTiO_3 below ~ 70 K the tetragonal symmetry is lowered and the Sr atoms are displaced along the [111] direction leading to the breaking of local inversion symmetry [19]. It is therefore possible that a (111) SrTiO_3 -based polar interface has such broken inversion symmetry in addition to conventional inversion symmetry breaking observed at polar oxide interfaces, which can result in an unconventional superconductivity. It has been recently suggested that dichalcogenide monolayers with hexagonal structure can be a realization of exotic Ising superconductivity where the spins are locked in an out-of-plane configuration due to the breaking of centro-symmetry [38–40]. We also note that the possibility for a nodless time-reversal-symmetry-breaking superconducting order parameter has been proposed for (111) SrTiO_3 -based interfaces from symmetry considerations [16].

In summary, the superconducting transition temperature T_c of the (111) $\text{LaAlO}_3/\text{SrTiO}_3$ interface has a nonmonotonic dependence on gate voltage. Maximum T_c is found at the same gate voltage where maximal values of spin-orbit field H_{SO} and spin-orbit energy ϵ_{SO} are observed. H_{SO} is extracted from weak antilocalisation while ϵ_{SO} is estimated from the superconducting properties. The $H_{c\parallel}$ exceeds the Chandrasekhar-Clogston limit by more than an order of magnitude due to strong spin-orbit interaction. We suggest that the crystalline spin-

orbit interaction becomes important close to an avoided band crossing region. In this regime orbital mixing can lead to enhanced spin-orbit interaction and superconductivity, which become weaker as V_g is tuned away from this avoided band crossing regime. This results in a dome in the spin-orbit energy (and T_c) versus V_g . However, a deeper insight to the link between spin-orbit interaction and the superconducting dome requires further development of theoretical models for this unique hexagonal oxide interface.

ide interface.

P.K.R. and E.M. contributed equally to this work. We are indebted to Moshe Goldstein and Alexander Palevski for useful discussions. This work has been supported by the Israel Science Foundation under grant 569/13, the Israel Ministry of Science technology and space under contract 3-11875 and the Bi-national science foundation under grant 2014047.

-
- [1] H. Y. Hwang, Y. Iwasa, M. Kawasaki, B. Keimer, N. Nagaosa, and Y. Tokura, *Nat. Mater.* **11**, 103 (2012).
- [2] A. Caviglia, S. Gariglio, N. Reyren, D. Jaccard, T. Schneider, M. Gabay, S. Thiel, G. Hammerl, J. Mannhart, and J.-M. Triscone, *Nature* **456**, 624 (2008).
- [S1] E. Maniv, M. B. Shalom, A. Ron, M. Mograbi, A. Palevski, M. Goldstein, and Y. Dagan, *Nat. Commun.* **6**, 8239 (2015).
- [4] M. Ben Shalom, M. Sachs, D. Rakhmievitch, A. Palevski, and Y. Dagan, *Phys. Rev. Lett.* **104**, 126802 (2010).
- [S2] A. D. Caviglia, M. Gabay, S. Gariglio, N. Reyren, C. Cancellieri, and J.-M. Triscone, *Phys. Rev. Lett.* **104**, 126803 (2010).
- [6] H. Liang, L. Cheng, L. Wei, Z. Luo, G. Yu, C. Zeng, and Z. Zhang, *Phys. Rev. B* **92**, 075309 (2015).
- [7] G. Herranz, F. Sánchez, N. Dix, M. Scigaj, and J. Fontcuberta, *Sci. Rep.* **2**, 758 (2012).
- [8] S. Davis, V. Chandrasekhar, Z. Huang, K. Han, Ariando, and T. Venkatesan, *Phys. Rev. B* **95**, 035127 (2017).
- [9] P. K. Rout, I. Agireen, E. Maniv, M. Goldstein, and Y. Dagan, *arXiv:1701.02153* (2017).
- [10] A. Monteiro, D. Groenendijk, I. Groen, J. de Bruijkere, R. Gaudenzi, H. van der Zant, and A. Caviglia, *arXiv:1703.04742* (2017).
- [11] S. Davis, Z. Huang, K. Han, Ariando, T. Venkatesan, and V. Chandrasekhar, *arXiv:1704.01203* (2017).
- [12] S. McKeown Walker, A. de la Torre, F. Y. Bruno, A. Tamai, T. K. Kim, M. Hoesch, M. Shi, M. S. Bahramy, P. D. C. King, and F. Baumberger, *Phys. Rev. Lett.* **113**, 177601 (2014).
- [13] T. C. Rödel, C. Bareille, F. Fortuna, C. Baumier, F. Bertran, P. Le Fèvre, M. Gabay, O. Hijano Cubelos, M. J. Rozenberg, T. Maroutian, et al., *Phys. Rev. Appl.* **1**, 051002 (2014).
- [14] D. Xiao, W. Zhu, Y. Ran, N. Nagaosa, and S. Okamoto, *Nat. Commun.* **2**, 596 (2011).
- [15] D. Doennig, W. E. Pickett, and R. Pentcheva, *Phys. Rev. Lett.* **111**, 126804 (2013).
- [16] M. S. Scheurer, D. F. Agterberg, and J. Schmalian, *npj Quantum Materials* **2**, 9 (2017).
- [17] S. Okamoto and D. Xiao, *arXiv:1705.05683* (2017).
- [18] K. A. Müller and H. Burkard, *Phys. Rev. B* **19**, 3593 (1979).
- [19] E. K. H. Salje, O. Aktas, M. A. Carpenter, V. V. Laguta, and J. F. Scott, *Phys. Rev. Lett.* **111**, 247603 (2013).
- [20] B. Chandrasekhar, *Appl. Phys. Lett.* **1**, 7 (1962).
- [21] A. M. Clogston, *Phys. Rev. Lett.* **9**, 266 (1962).
- [22] R. A. Klemm, A. Luther, and M. Beasley, *Phys. Rev. B* **12**, 877 (1975).
- [23] Y. Nakamura and Y. Yanase, *J. Phys. Soc. Jpn.* **82**, 083705 (2013).
- [24] A. Smink, J. de Boer, M. Stehno, A. Brinkman, W. van der Wiel, and H. Hilgenkamp, *Phys. Rev. Lett.* **118**, 106401 (2017).
- [25] G. Singh, A. Jouan, L. Benfatto, F. Couedo, P. Kumar, A. Dogra, R. Budhani, S. Caprara, M. Grilli, E. Lesne, et al., *arXiv:1704.03365* (????).
- [26] J. Biscaras, N. Bergeal, S. Hurand, C. Grossetête, A. Rastogi, R. Budhani, D. LeBoeuf, C. Proust, and J. Lesueur, *Phys. Rev. Lett.* **108**, 247004 (2012).
- [27] See Supplemental Material for more details about two band model for Hall data and the analysis of weak antilocalisation.
- [28] For $V_g \leq -40$ V the saturation resistance at high field is significantly larger than the resistance at 350mK (above T_c). But these two quantities coincide for other gate voltages. This may be related to the proximity to a superconductor-to-insulator transition for lower V_g and will be discussed elsewhere.
- [29] G. Herranz, G. Singh, N. Bergeal, A. Jouan, J. Lesueur, J. Gázquez, M. Varela, M. Scigaj, N. Dix, F. Sánchez, et al., *Nat. Commun.* **6**, 6028 (2015).
- [30] S. Maekawa and H. Fukuyama, *Journal of the Physical Society of Japan* **50**, 2516 (1981).
- [31] M. B. Shalom, A. Ron, A. Palevski, and Y. Dagan, *Phys. Rev. Lett.* **105**, 206401 (2010).
- [32] S. Lerer, M. B. Shalom, G. Deutscher, and Y. Dagan, *Physical Review B* **84**, 075423 (2011).
- [33] D. Rainer and G. Bergmann, *Physical Review B* **32**, 3522 (1985).
- [34] I. Žutić, J. Fabian, and S. Das Sarma, *Rev. Mod. Phys.* **76**, 323 (2004).
- [35] Z. Zhong, A. Tóth, and K. Held, *Phys. Rev. B* **87**, 161102 (2013).
- [36] K. Michaeli, A. C. Potter, and P. A. Lee, *Phys. Rev. Lett.* **108**, 117003 (2012).
- [37] H. Shimahara, *Journal of the Physical Society of Japan* **66**, 541 (1997).
- [38] J. Lu, O. Zheliuk, I. Leermakers, N. F. Yuan, U. Zeitler, K. T. Law, and J. Ye, *Science* **350**, 1353 (2015).
- [39] X. Xi, Z. Wang, W. Zhao, J.-H. Park, K. T. Law, H. Berger, L. Forró, J. Shan, and K. F. Mak, *Nat. Phys.* **12**, 139 (2016).
- [40] Y. Saito, Y. Nakamura, M. S. Bahramy, Y. Kohama, J. Ye, Y. Kasahara, Y. Nakagawa, M. Onga, M. Tokunaga, T. Nojima, et al., *Nat. Phys.* **12**, 144 (2016).

SUPPLEMENTAL MATERIAL

S1. TWO BAND ANALYSIS OF HALL DATA

We have analysed the Hall data (Fig. S1) using a simplified two band model with no interaction effects. As discussed in the manuscript, one of them should be a hole band while the other is a electron band. In this model, the low field Hall coefficient is given as:

$$R_H = \frac{1}{e} \frac{n_h \mu_h^2 - n_e \mu_e^2}{(n_h \mu_h + n_e \mu_e)^2}. \quad (\text{S1})$$

where $n_{h(e)}$ and $\mu_{h(e)}$ are hole (electron) carrier density and mobility, respectively. The corresponding sheet resistance at zero magnetic field is $R_S = [e(n_h \mu_h + n_e \mu_e)]^{-1}$. For relatively small V_g range used, the nonlinearities in the dielectric constant can be neglected and the change in total carrier density for change in V_g (ΔV_g) can be given as: $C_{STO} \Delta V_g = e(\Delta n_h + \Delta n_e)$, where C_{STO} is the capacitance of STO (111) per unit area. The corresponding changes in $n_{h(e)}$ are proportional to effective masses $m_{h(e)}$ for parabolic bands and therefore $\Delta n_h / \Delta n_e = m_h / m_e$. We have assumed $m_h = m_e$ for our calculations. Using all these expressions, we have extracted $n_{h(e)}$ and $\mu_{h(e)}$ [See Fig. S1 (a,b)].

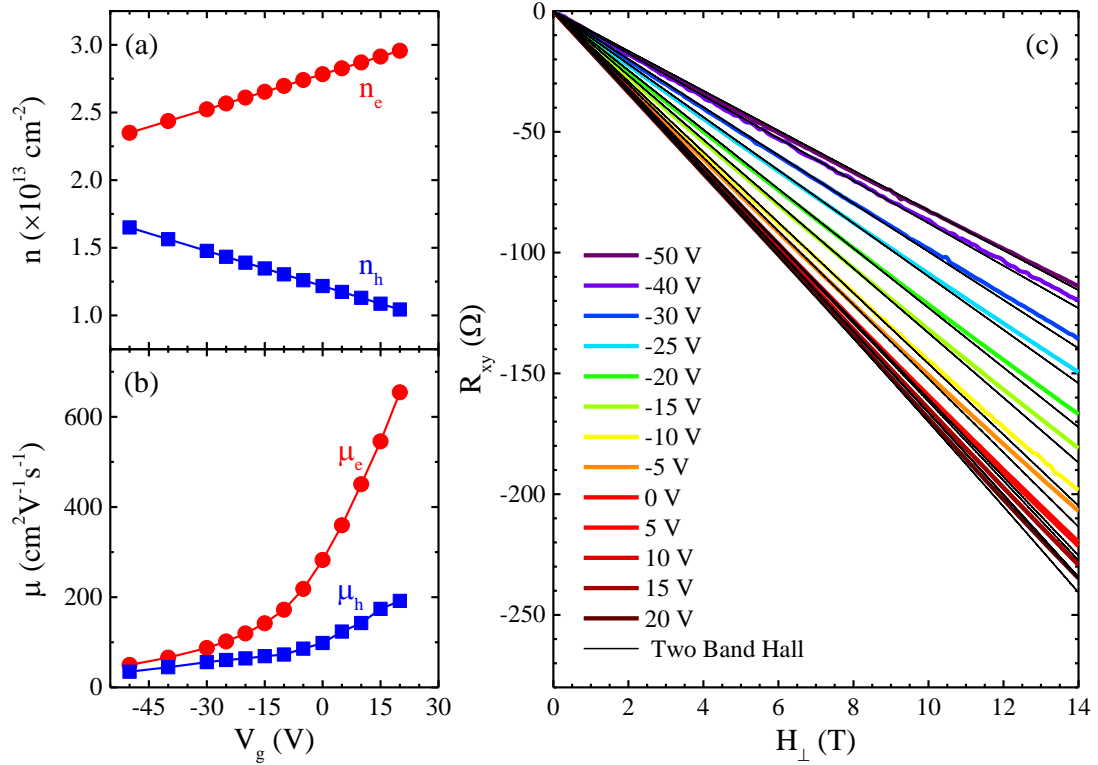


FIG. S1. The gate dependance of carrier density (a) and mobility (b) for electron and hole band extracted from two band model. (c) The Hall resistance (R_{xy}) as a function of magnetic field for different V_g measured at 5 K. The solid curves are plotted using the extracted $n_{h(e)}$ and $\mu_{h(e)}$ in Eq. S2.

Using the extracted $n_{h(e)}$ and $\mu_{h(e)}$, we have calculated the Hall resistance for high magnetic fields by the expression:

$$R_{xy} = \frac{1}{e} \frac{(n_h \mu_h^2 - n_e \mu_e^2) + \mu_h^2 \mu_e^2 (n_h - n_e) H^2}{(n_h \mu_h + n_e \mu_e)^2 + \mu_h^2 \mu_e^2 (n_h - n_e)^2 H^2} H. \quad (S2)$$

The calculated Hall curves have good agreement with the measured data for lower fields [See Fig. S1 (c)]. However, we see more deviation with increasing field. This can be due to more complicated effects such as splitting of the electron band into two spin states with an avoided band crossing due to spin-orbit interaction. Our simplified two-band description cannot capture these effects. We want to point out that, in order to perform a more accurate analysis, one needs additional measurements such as Shubnikov-de Haas oscillations, which can accurately determine the carrier density in the mobile band [S1]. Despite its simplicity our analysis provides the parameter regimes for the electron and hole bands and the qualitative trend of these parameters.

As expected, n_e increases with increasing V_g while n_h follows the opposite trend [See Fig. S1 (a)]. However, the mobility increases with V_g for both bands. The drastic rise in mobility μ_e with increasing V_g can be responsible for large variation in R_S . Since $n_e \mu_e^2 > n_h \mu_h^2$ for all V_g , Eq. S1 reveals that the Hall slope should be negative as observed in Fig. S1 (c). Therefore $1/|eR_H|$ starts increasing with increasing V_g (or increasing number of electrons).

S2. ANALYSIS OF MAGNETORESISTANCE DATA

Figure S2 presents gate dependence of g -factor as well as the coefficients A and C related to orbital magnetoresistance given by the last term in Eq. (1) of the manuscript. According to Drude model for a two-dimensional electron gas, the elastic scattering time τ is given by $\tau = m^*/e^2 n_S R_S$ (m^* is the effective electron mass and n_S is the carrier density) and the diffusion coefficient D can be expressed as: $D = v_F^2 \tau / 2$ ($v_F = \hbar \sqrt{2\pi n_S} / m^*$ is the Fermi velocity). We have extracted D for various V_g and used it for the fitting of magnetoresistance data [Fig. 3 in the manuscript]. The extracted g values are slightly higher than the typical values of 2 for a free electron system and slowly increase with increasing V_g . Similar gate dependence of g has been observed in (100) interface previously [S2]. A and C are related to the mobility (μ) and as expected increases with μ when the gate voltage V_g is increased. However, the exact dependencies of these parameters on other measurable transport parameters (like R_S , n_S etc.) are much more complicated due to multiband charge transport.

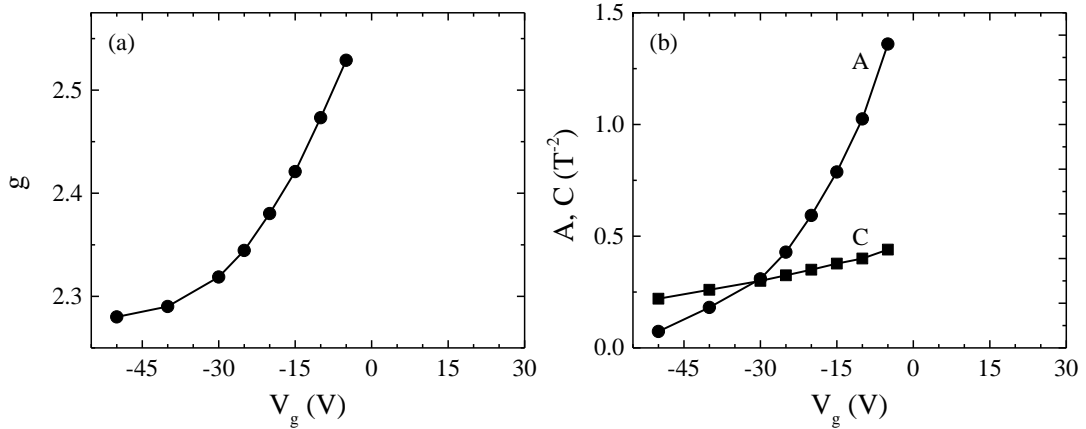


FIG. S2. Gate dependence of the fitting parameters g (a), A (b) and C (b) at 1.3 K.

We can determine the spin-orbit time τ_{SO} and the inelastic time τ_i using the relations $H_{i,SO} = \hbar/4eD\tau_{i,SO}$. Therefore, we can determine τ_{SO} , τ_i , and τ using the experimental values of R_S , n_S (or $1/|eR_H|$), the fitting parameters H_i , H_{SO} , and a typical $m^* = 3m_e$ (m_e is the electronic mass). These three time scales are presented in Fig. 3(d) of the manuscript.

[S1] E. Maniv *et al.*, Nat. Commun. **6**, 8239 (2015).

[S2] A. D. Caviglia *et al.*, Phys. Rev. Lett. **104**, 126803 (2010).